Values of the intrinsic quadrupole moment can be obtained from spectroscopic and from Coulomb excitation data. Using the expression $E_m=79.7A^{-\frac{1}{3}}$ to give the mean energy for the giant resonance and measured values of the quadrupole moments, the energies E_a and E_b can be calculated from the above expressions. The results of several such calculations are given in Table II. If the intrinsic widths associated with the two axes are assumed to be the same as that for an undeformed nucleus, i.e., approximately 4 Mev, the half-maximum points would be expected to occur about 2 Mev below E_a and 2 Mev above E_b. The last two columns of Table II give the half-maximum points obtained from Fig. 5. In comparing these energies it should be pointed out that the value of $E_{\frac{1}{2}}^+$ will depend much more critically on the correction made for neutron multiplicity than will the value of $E_{\frac{1}{2}}^-$. The values of E_a and E_b calculated from the Coulomb-excitation-derived quadrupole moments are in reasonable agreement with the half-maximum energies found in this experiment. Since the large quadrupole moments obtained from the spectroscopic measurements give values of E_a less than the half-maximum energy $E_{\frac{1}{2}}^-$, these moments are in disagreement with the widths obtained for these giant resonances.

ACKNOWLEDGMENTS

The authors wish to thank M. Danos and J. E. Leiss for many fruitful discussions.

PHYSICAL REVIEW VOLUME 112, NUMBER 2 OCTOBER 15, 1958

Splitting of the Giant Resonance for Deformed Nuclei*

E. G. FULLER AND M. S. WEISS†
National Bureau of Standards, Washington, D. C.
(Received June 16, 1958)

Photoneutron yield measurements have been made for terbium, tantalum, and gold with good energy resolution from threshold up to 25 Mev. Neutron-production cross sections were obtained directly from the experimental points without smoothing the raw data. Corrections were made for the multiple production of neutrons above the $(\gamma,2n)$ thresholds. The giant resonances for terbium and tantalum were found to be split into two resonances as predicted by Okamoto and Danos. The giant resonances for all three nuclei were fitted by the superposition of two Lorentz shape resonance lines. The intrinsic quadrupole moments determined from these fits to the experimental data were: terbium, $+5.6\pm0.6$ barns; tantalum, $+5.7\pm0.3$ barns; and gold, $+1.6\pm0.6$ barns.

1. INTRODUCTION

THE giant resonances of closed-shell nuclei have been observed to be appreciably narrower than those of nuclei situated between closed shells.[1] Previous work[2] in this laboratory indicated that the giant resonances of the rare-earth nuclei were larger than any previously observed. While not established by that experiment, the data obtained for terbium, holmium, erbium, ytterbium, and tantalum were consistent with the giant resonance for these nuclei being split into two peaks. These results were all in accord with the predictions of Okamoto[3] and Danos[4] that the giant resonance for a deformed nucleus should be split into two resonances. The extension of the hydrodynamical model for the nuclear photoeffect[5] made by Okamoto and Danos leads to a giant resonance energy being associated with each of the axes of a deformed nucleus.[3-4]

It was the object of the present work to examine with good energy resolution the details of the shape of the giant resonance for two highly deformed nuclei and of one having a considerably smaller deformation to see if the details of the resonance shapes for such nuclei would confirm the predictions of Danos.[6] The nuclei terbium, tantalum, and gold were chosen for study[7] because they were available in moderate quantities in monoisotopic form.

* This work supported by U. S. Atomic Energy Commission.
† On educational leave at Massachusetts Institute of Technology, Cambridge, Massachusetts.
[1] R. Nathans and J. Halpern, Phys. Rev. **93**, 437 (1954); R. Nathans and P. J. Yergin, Phys. Rev. **98**, 1296 (1955).
[2] Fuller, Petree, and Weiss, Phys. Rev. **112**, 554 (1958), preceding paper.
[3] K. Okamoto, Progr. Theoret. Phys. Japan **15**, 75 (1956); Phys. Rev. **110**, 1113 (1958).
[4] M. Danos, Bull. Am. Phys. Soc. Ser. II, **1**, 135 (1956).
[5] M. Goldhaber and E. Teller, Phys. Rev. **74**, 1048 (1948); J. H. D. Jensen and P. Jensen, Z. Naturforsch. **5a**, 343 (1950).
[6] M. Danos, Nuclear Phys. **5**, 23 (1958).
[7] Some of the preliminary results of this experiment were reported at the Stanford Conference on Nuclear Sizes and Density Distributions [G. M. Temmer, Revs. Modern Phys. **30**, 498 (1958)]. In agreement with these results B. M. Spicer (private communication) has also observed the splitting of the neutron production cross section for tantalum. These data were analyzed by smoothing the experimental activation curve. The authors want to thank Dr. Spicer for sending them his preliminary results.

2. EXPERIMENTAL DETAILS

Good energy resolution as used for this experiment meant that the activation curve data were taken at the proper intervals and with sufficient statistical accuracy to make possible the calculation of a statistically significant cross section directly from the experimental data without recourse to any smoothing procedures. This required that somewhere between one-half and one and one-half million counts be recorded at each point on the activation curve. The feasibility of carrying out such an experiment was shown when, in the course of the measurements of the tip shape of the bremsstrahlung spectrum, it was found possible to maintain the stability of the betatron's energy to within 20 kev for periods of several months.[8] The only additional requirement was that the neutron-detecting equipment be stable within the limits set by the counting statistics. It was found possible to achieve this stability with conventional equipment.

Except for some rather minor modifications, the experimental arrangement and procedure used for this experiment was the same as that used in the previous survey experiment.[2] The only change in the electronics was to divide the ten BF_3 counters used in the detector into four channels. Two of these channels consisted of three counters, and two had two counters, connected in parallel. Each of the four channels had its own preamplifier, amplifier, gate, discriminator, and scaler. This arrangement permitted higher counting rates than would have been acceptable with all 10 counters connected in parallel. With a counting rate of 25 600 counts per minute, counting rate losses were found to be three percent. Except near threshold, data were taken at about half of this rate. Counting-loss corrections were applied to all measured yields. These corrections were determined from yields of 0.1% statistical uncertainty $(1/\sqrt{n})$ measured at a given energy as a function of counting rate.

During the course of the experiment a number of checks were made of the stability of the various components used to make the measurements. The quantities checked were the neutron detection efficiency, the sensitivity of the transmission ionization chamber, the stability of the gating circuit, and the energy of the betatron. The neutron detection efficiency was checked daily by observing the counting rate when a Ra-Be (α,n) neutron source was placed inside the detector. These counting rates were measured to 0.3% statistical uncertainty. Corrections were made for the small drifts observed in this rate. Drifts were less than 1.5%.

The transmission ionization chamber used in these measurements was not sealed. Its sensitivity then varied slightly with the density of the air in the chamber. The over-all beam-monitoring system was checked regularly by determining the time necessary to collect a given charge from the ionization chamber when a Co^{60} source was placed at a standard position with respect to the ionization chamber. The corrections for the changes in the monitor sensitivity were usually of the order of $\pm 0.5\%$.

The stability of the betatron's energy control and of the gating circuits were frequently examined by measuring the neutron yield from copper at an arbitrary point on its activation curve. These data indicated that any shifts in the betatron's energy calibration, during the two-month period over which the data were taken, were less than 50 kev. The data were not inconsistent with the indications found during the measurements of the bremsstrahlung tip shape that the energy of the betatron was stable to less than ± 20 kev.

The samples from which the neutron yields were measured were a gold disk 3.54 g/cm^2 thick and 3.8 cm in diameter, a tantalum disk 3.53 g/cm^2 thick and 4 cm in diameter, and 3 grams of Tb_4O_7 in a plastic cylinder 1.4 cm in diameter and 1.5 cm in length. Target-out backgrounds amounted to less than 0.5% in all cases. The neutron yield from a water sample was also measured and used to correct the Tb_4O_7 data for the oxygen present in the sample. This correction was less than 4% at all energies.

The total neutron yield from each of the samples was measured as a function of the peak energy in the bremsstrahlung spectrum from the (γ,n) threshold up to 25 Mev. Data were taken every 500 kev at the integer and half-integer Mev points. In addition data were taken on the quarter- and on the three-quarter-Mev points for tantalum in the energy region from threshold up to 19.5 Mev. The activation curve for each sample was measured many times during the period during which data were taken. For each of the samples these measurements were all consistent with each other within the statistical errors of the individual points. The individual determinations of the activation curve for each sample were then averaged to obtain a final activation curve for each sample. In the case of gold and tantalum, the total number of counts accumulated varied from about 4×10^5 counts in the region around 13 Mev to about three times that number at 19 Mev. In the case of terbium, the numbers were about one-fifth of these. The first differences of the final averaged yield curves are shown in Figs. 1–3. The differences are taken over half-Mev intervals. The indicated errors are the statistical uncertainties in these first differences.

3. ANALYSIS OF THE DATA

The quantity measured in this experiment is the total photoneutron yield as a function of the peak energy, E_0, in the bremsstrahlung spectrum. If $Y(E_0)$ represents this quantity normalized to the total number of Mev in the bremsstrahlung spectrum that would have been incident on the sample if there were no absorption of photons between the betatron target and

[8] Fuller, Hayward, and Koch, Phys. Rev. **109**, 630 (1958).

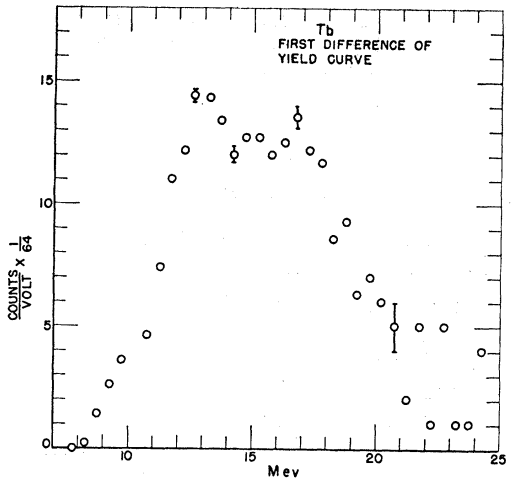

FIG. 1. First difference of terbium activation curve. First differences were taken over half-Mev intervals.

the sample, then $Y(E_0)$ will be given by

$$Y(E_0)=\int_0^{E_0} I(E,E_0)\Omega(E)dE. \quad (1)$$

In this expression $I(E,E_0)$ represents the differential intensity spectrum of the bremsstrahlung (Mev per Mev) and $\Omega(E)$ is the "reduced neutron-production cross section." In terms of the actual total neutron-production cross section, $\sigma_{Tn}(E)$, $\Omega(E)$ is given by

$$\Omega(E)=\frac{\sigma_{Tn}(E)}{E}\rho\left(\frac{1-e^{-tx}}{t(E)}\right)e^{-L(E)}, \quad (2)$$

where ρ is the density (atoms per cm^3) of the sample, x is the length of the sample, $t(E)$ the electronic absorption coefficient in the sample, and $L(E)$ is the number of mean free paths of absorbing material between the betatron target and the sample. In the case of terbium, $\Omega(E)$ must also include a factor giving the ratio of the sample area to the area of the bremsstrahlung beam at the sample position. For gold and tantalum the sample diameters were greater than the beam diameter at the exposure position.

With the proper normalization of the experimental data points, $Y(E_0)$, the Penfold-Leiss[9] inverse bremsstrahlung matrix can be used to solve for $\Omega'(E_i)$. It has been shown[9] that $\Omega'(E_i)$ is related to $\Omega(E)$ by an expression of the form:

$$\Omega'(E_i)=\int_0^{E_i+\frac{1}{2}\Delta E} T(E,E_i+\tfrac{1}{2}\Delta E)\Omega(E)dE. \quad (3)$$

In this expression ΔE is the interval between the data points, $Y(E_0)$, used to obtain $\Omega'(E_i)$. Penfold and Leiss have shown that over the final interval from $(E_i-\frac{1}{2}\Delta E)$ to $(E_i+\frac{1}{2}\Delta E)$, T has the shape of the high-energy tip of the bremsstrahlung spectrum. Below $(E_i-\frac{1}{2}\Delta E)$ it oscillates about the value zero. In a manner which will be described below, the quantity $\Omega'(E_i)$ can be corrected to give the approximate value of the smooth function $\Omega(E)$ at the energy E_i.

All of the data of this experiment were analyzed with ΔE equal to one Mev. This procedure was a result of a compromise between the energy resolution desired for the final cross section and the magnitude of the error in the final cross section resulting from the statistical uncertainties in the original data points, $Y(E_0)$. In all cases the inverse matrix of Penfold and Leiss was applied directly to experimental data after suitable corrections were made for backgrounds and for the oxygen content of the terbium sample. No attempt was made to smooth any of the experimental data. Since the activation curves for terbium and gold were measured at half-Mev intervals, the data were used to make two independent determinations of the cross sections for these nuclei. For tantalum, where data were taken every quarter Mev, four independent determinations were made of the cross section. In Figs. 5 to 7, these determinations are indicated by circles, triangles, and dots. The errors shown are the result of propagating the statistical errors of the experimental data, $\sqrt{n}$, through the inverse bremsstrahlung matrix.

The data actually plotted in Figs. 6 to 8 were obtained in the following way. The inverse bremsstrahlung matrix was first applied to the experimental data to obtain $\Omega'(E_i)$. A smooth curve was drawn through these points. This curve, $\Omega^*(E)$, was taken as an approximation for the true curve $\Omega(E)$. Using $\Omega^*(E)$ and the weighting function $T(E, E_i+\frac{1}{2}\Delta E)$, $\Omega''(E_i)$ was calculated at a number of points. This average was then compared with the value of the smooth function $\Omega^*(E)$ at the energy E_i to obtain the ratio of $\Omega^*(E)$ at E_i to the average of $\Omega^*(E)$ weighted with T. This ratio was applied to the value of $\Omega'(E_i)$ derived from the experimental data as a correction for the effect of the weighting function and the width of the bin used in the analysis. This correction amounted to a maximum of 5% in the case of the relatively sharp-peaked data obtained from tantalum. The points obtained in this way were assumed to define the smooth function $\Omega(E)$. These points were then corrected by means of Eq. (2) to give the smooth cross section $\sigma_{Tn}(E)$. Above the $(\gamma,2n)$ threshold a correction was then applied for the neutron multiplicity (to be discussed in a later section). Within the approximations indicated above, the points plotted in Figs. 5 to 7 represent the smooth cross section $\sigma_n(E)=\sigma(\gamma,n)+\sigma(\gamma,2n)+\sigma(\gamma,pn)+\cdots$.

4. DISCUSSION OF THE ANALYSIS

Before discussing the significance of the cross sections given in Figs. 5 to 7, some consideration should be

[9] A. S. Penfold and J. E. Leiss, Phys. Rev. 95, 637(A) (1954) and private communication; also, *Analysis of Photo Cross Sections* (Physics Research Laboratory, University of Illinois, Champaign, Illinois, 1958).

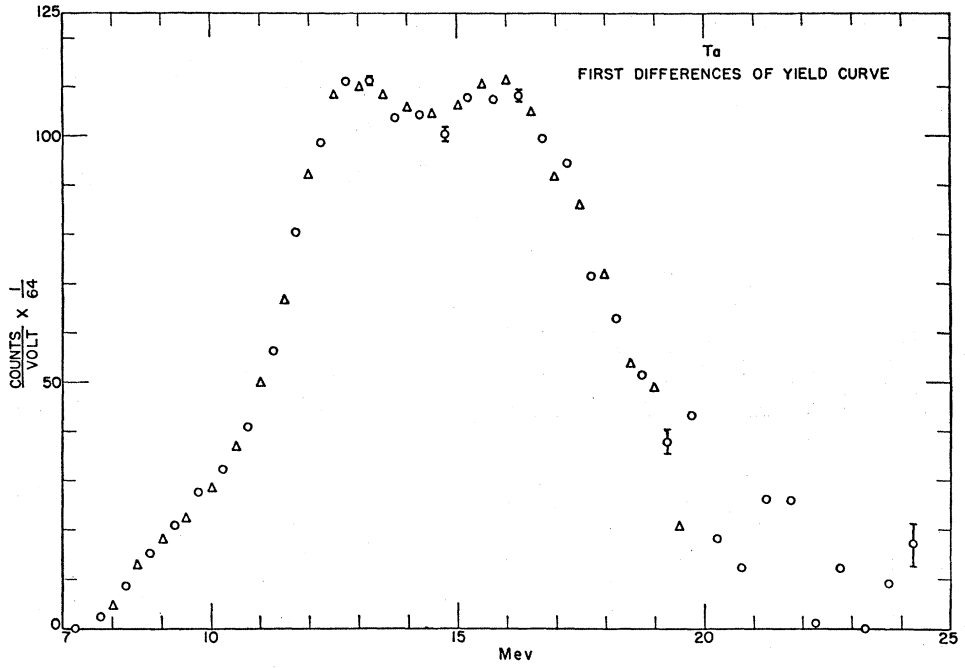

FIG. 2. First differences of tantalum activation curve. First differences were taken over half-Mev intervals. The circles and triangles represent independent determinations of the first differences of the original activation curve data.

given to the validity of the various factors that went into the calculation of the cross sections. The general feature of the two peaks in the cross section for terbium and tantalum, and the single peak for gold cannot result from these factors. Details of the shape of the cross section, however, can be strongly influenced by them. The points in question are the response of the transmission-chamber monitor as a function of bremsstrahlung energy, the use by Penfold and Leiss of the "Schiff integrated-over-angle" spectrum in calculating the inverse matrix, the absolute determination of the monitor response, the neutron-detection efficiency as a function of energy, and the calculation of the neutron multiplicity.

Of the above factors, the monitor response as a function of energy will have the most effect on the details of the shapes of these cross sections. To a considerably lesser extent, the assumed spectral shape (use of the Penfold-Leiss tables) will also affect these shapes. The monitor response used was based on a calibration made by the scintillation spectrometer method.[10] This calibration was made at bremsstrahlung energies of 6, 8, 10, 13, 19, and 27 Mev. At each energy the calibration was felt to be known to about 5%. A curve drawn through these points and smoothed to five significant figures was used in analyzing these data. A number of indirect checks are available on the validity of the use of these factors: First, a check was obtained by measuring the neutrons produced by the photodisintegration of deuterium from a heavy water sample. The neutron yield was measured at 6, 8, 10, 13, 16, and 19 Mev. The ratio of the calculated to the observed yield was constant to within 1% between 10 and 16 Mev and to

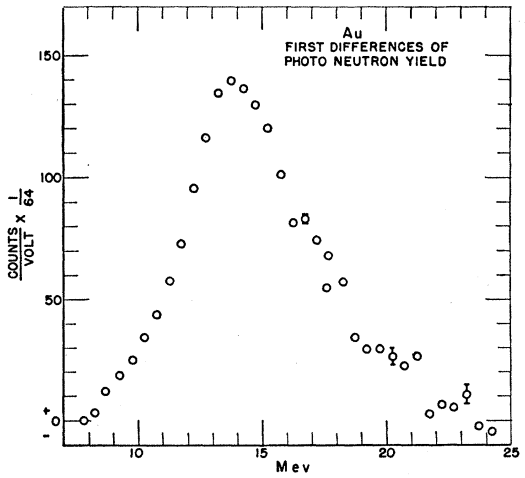

FIG. 3. First differences of gold activation curve. First differences were taken over half-Mev intervals.

[10] Koch, Leiss, and Pruitt, Bull. Am. Phys. Soc. Ser. II, 1, 199 (1956). The calibration used was one made by one of us (EGF) using the betatron. Later work in this laboratory, both with a calorimeter and using the scintillation counter method seems to indicate that this calibration may be in error for energies above 18 Mev. If the new calibration is used to analyze the data for this experiment, the cross sections obtained above 18 Mev would be lower than those plotted in Figs. 5–7 by an amount that would increase to about 20% at 24 Mev.

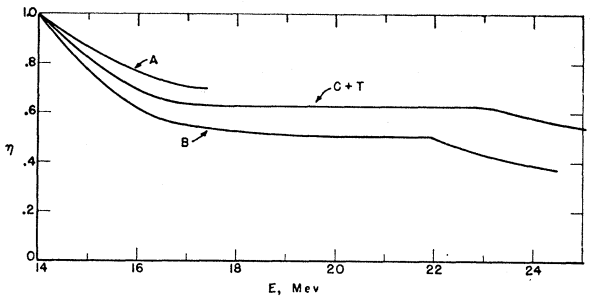

FIG. 4. Reciprocal neutron multiplicities. The curve labeled $C+T$ was calculated from the cross sections given by Carver and Turchinetz (reference 16). Curves labeled A and B are estimates of the limits on this function. Curve B is calculated from the $\sigma(\gamma,2n)$ cross section given in Blatt and Weisskopf (reference 13).

within 4% over the range from 6 to 19 Mev.[11] The absolute efficiency of the neutron detector calculated from the deuterium data was 8% less than that obtained with the calibrated Ra-Be (α,n) neutron source after correcting its counting rate for the distribution of neutron counts within the gate used for the photoneutron measurements. Considering the uncertainties in the neutron source strength and the absolute deuterium photodisintegration cross section, this difference is not thought to be significant. Second, in the measurements made of the shape of the tip of the bremsstrahlung spectrum from this betatron,[8] it was shown that at 15 Mev this shape was very well described by the Schiff spectrum to within 100 kev of the end of the spectrum. Third, these data also showed that, to within the experimental errors of about 10%, the Schiff spectrum and the monitor response described above gave the correct ratio for the relative number of 15.11-Mev photons in a 16-Mev spectrum to those in a 38-Mev spectrum.

A check on the absolute cross section measurements and to some extent on the shape of the cross sections can also be made by using the dipole dispersion relation to calculate the elastic scattering cross section from the cross section for the giant resonance obtained in this measurement.[12] This check is based on the assumption that the neutron cross section, $\sigma_n=\sigma(\gamma,n)+\sigma(\gamma,2n)+\sigma(\gamma,pn)+\cdots$, obtained in this sort of experiment gives the total photon absorption cross section. Since the scattering cross section is related to the square of this absorption cross section, the agreement of the calculated scattering cross section with even the rather poorly measured scattering cross sections indicates that the absorption cross sections are known to within 10%.

Above the $(\gamma,2n)$ threshold, the shape of the cross sections given in Figs. 5 to 7 are strongly dependent on the function used to correct for neutron multiplicity.

[11] For this comparison the cross section for the photodisintegration of the deuteron given by L. Hulthén and B. C. H. Nagel was used [Phys. Rev. **90**, 62 (1953)].

[12] E. G. Fuller and E. Hayward, Phys. Rev. **101**, 692 (1956). These comparisons have been made by fitting Lorentz lines to the gold data obtained in this work and to the tin, iodine, gold, and lead data obtained in the survey experiment.

TABLE I. Resonance parameters.

	Tb^{159}	Ta^{181}	Au^{197}
B_{2n} (Mev)	15.2	14.0	14.2
E_a (Mev)	12.5	12.45	13.15
σ_a^0 (Mb)	258	308	255
Γ_a (Mev)	2.4	2.3	2.9
E_b (Mev)	16.3	15.45	13.90
σ_b^0 (Mb)	310	348	365
Γ_b (Mev)	4.0	4.4	4.0

This function can be calculated in the statistical model. There is, however, a considerable amount of experimental evidence that not all of the particles emitted from a nucleus as the result of the absorption of a photon can be described by a statistical "boiling off" process. Particularly in the region above the peak of the giant resonance, there is some indication that a relatively large fraction of the photons absorbed may result in a so-called "direct effect," i.e., the emission of a particle with such a high energy that it is impossible for the nucleus to emit a second particle. The result is that the use of the statistical model as given by Blatt and Weiskopf[13] to calculate the neutron multiplicity results in an overestimate of this effect.

Fortunately, there is a rather large amount of rather consistent experimental data from various laboratories that can be used to determine the neutron multiplicity for tantalum. The neutron multiplicity is defined as

$$m=\frac{\sigma_{Tn}}{\sigma_n}=\frac{\sigma(\gamma,n)+2\sigma(\gamma,2n)+\sigma(\gamma,pn)+3\sigma(\gamma,3n)+\cdots}{\sigma(\gamma,n)+\sigma(\gamma,2n)+\sigma(\gamma,pn)+\sigma(\gamma,3n)+\cdots}. \quad (4)$$

On the statistical model it would be expected that for a heavy nucleus like tantalum, m would approach the value two approximately 5 Mev above the $(\gamma,2n)$ threshold and remain at this value until the $(\gamma,3n)$ threshold was reached. Both the data of Hanson and Whalin[14] and that of Carver, Edge, and Lokan[15] indicate that m approaches a value of about 1.7. These data indicate that for energies above the peak of the giant resonance a rather large portion of the photons absorbed by the tantalum nucleus go into the production of "fast neutrons." The fraction of "fast neutrons" produced by photons in the 14- to 16-Mev range as given by the cross sections found by Carver and Turchinetz[16] is in good agreement with the fraction

[13] J. M. Blatt and V. F. Weisskopf, *Theoretical Nuclear Physics* (John Wiley and Sons, Inc., New York, 1952), p. 379.

[14] E. A. Whalin and A. O. Hanson, Phys. Rev. **89**, 324 (1953).

[15] Carver, Edge, and Lokan, Proc. Phys. Soc. (London) **A70**, 415 (1957).

[16] J. H. Carver and W. Turchinetz, Proc. Phys. Soc. (London) **71**, 613 (1958). Their original data did not show any indication of two peaks in the total neutron cross section for tantalum. Recent measurements by Carver and Turchinetz [Photonuclear Conference, Washington, D. C., April 30 and May 1, 1958 (unpublished report)] have shown that the total neutron cross section for tantalum is split into two peaks.

given by Bertozzi[17] as a result of his measurements of the photoneutron spectra produced by photons in this energy range.

The tantalum data from this experiment were corrected for the neutron multiplicity by using a function that was calculated from the cross section given by Carver and Turchinetz. This function, labeled $C+T$ in Fig. 4, is just the reciprocal of the neutron multiplicity defined by Eq. (4). The curve labeled B is that obtained using the expression for the $(\gamma,2n)$ cross section given by Blatt and Weisskopf. Curve A is a guess as to what an extreme limit might be for this function on the high side of the curve calculated from the data of Carver and Turchinetz. For gold and terbium it was assumed that the neutron multiplicity was the same function of the energy above the $(\gamma,2n)$ threshold as it was in the case of tantalum. The $(\gamma,2n)$ thresholds used were calculated from the empirical mass equation of Levy.[18] These thresholds are given in Table I.

5. DISCUSSION OF THE RESULTS

The data given in Figs. 1 to 3 and Figs. 5 to 7 indicate that, in agreement with the predictions of Okamoto[3] and Danos,[4] the giant resonances for the highly deformed nuclei, terbium and tantalum, are split into two peaks. Danos[6] has shown that on a simple hydrodynamical model of the nucleus, it should be possible to fit these giant resonances by the superposition of two Lorentz shape "resonance lines," i.e., a cross section given by an expression of the form:

$$\sigma_n=\frac{\sigma_a}{1+[(E^2-E_a^2)/E\Gamma_a]^2}+\frac{\sigma_b}{1+[(E^2-E_b^2)/E\Gamma_b]^2}. \quad (5)$$

For a nucleus that is a prolate spheroid the area under the high-energy line should be approximately twice the area under the low-energy line.[6]

The smooth curves drawn in Figs. 5 to 7 are "best fits by eye" to the experimental data made with the aid of an analog computer set up to plot the superposition of two Lorentz lines. In making these fits, an approximate (within 10%) two-to-one area ratio was imposed on the two resonance lines. In the case of terbium, little can be said about the fit as a result of the poor statistics. In the case of tantalum, it was not possible to maintain the two-to-one area ratio and at the same time fit the experimental data below the $(\gamma,2n)$ threshold if the neutron multiplicity given by the data of Carver and Turchinetz was used. The curve given in Fig. 6 comes closest to agreeing with this multiplicity and at the same time maintaining the two-to-one ratio. In the case of gold, a considerably better fit was obtained to the experimental points, particularly in the region of the peak and leading edge of the reso-

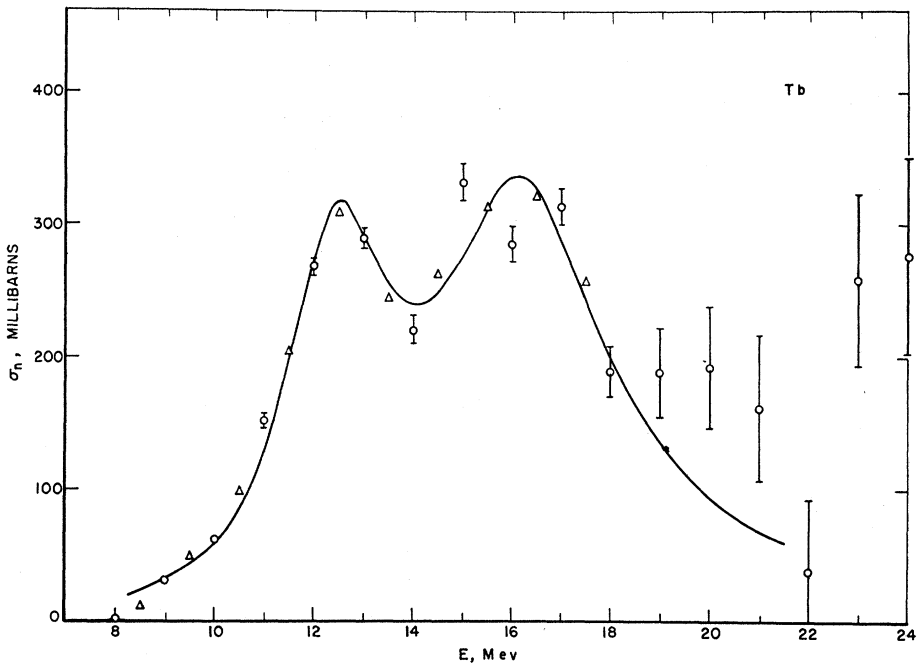

FIG. 5. Neutron cross section for terbium. Circles and triangles represent independent determinations of the cross section from the original data. Errors represent standard deviations based on the statistical uncertainties ($\sqrt{n}$) in the original activation curve data. The cross section plotted is $\sigma_n=\sigma(\gamma,n)+\sigma(\gamma,2n)+\sigma(\gamma,pn)+\cdots$. The smooth curve is calculated from the parameters given in Table I by using Eq. (5).

[17] W. Bertozzi, Ph.D. thesis, Massachusetts Institute of Technology, 1958 (unpublished); Bertozzi, Paolini, and Sargent, Phys. Rev. **110**, 790 (1958).
[18] H. B. Levy, Phys. Rev. **106**, 1265 (1957).

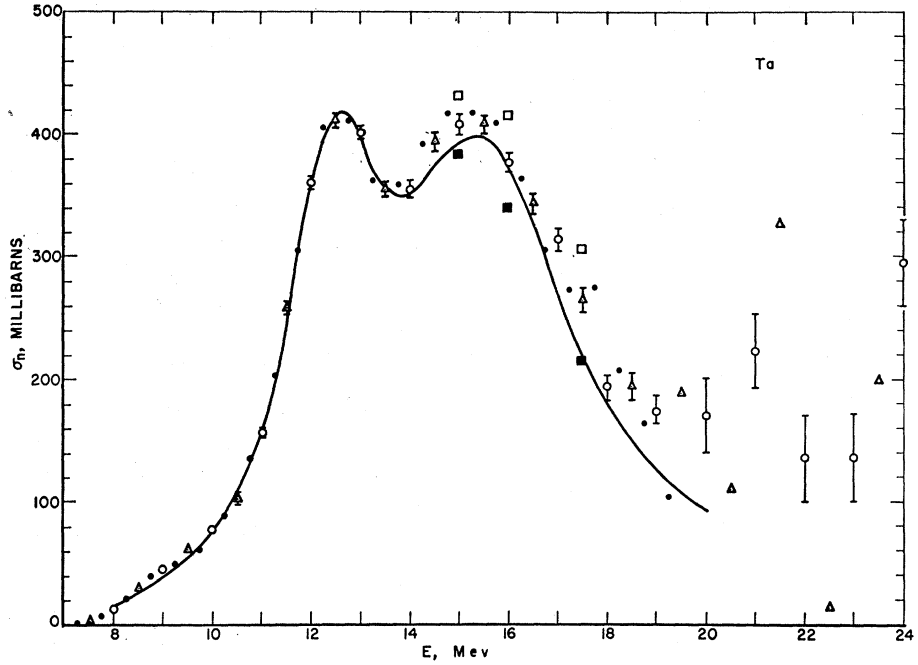

FIG. 6. Neutron cross section for tantalum. See Fig. 5 for description. Circles, triangles, and alternate dots represent four independent determinations of the cross section from the original activation curve. The correction for neutron multiplicity required to bring the experimental points down to the smooth curve in the region from 14 to 16 Mev would probably be within the limits of errors on the cross sections given by Carver and Turchinetz (reference 16). The open squares and closed squares correspond to the limiting positions of the experimental points based on curves A and B given in Fig. 4.

nance, if a superposition of two Lorentz lines was used to fit the data rather than a single broader line. The parameters for the curves plotted in Figs. 5 to 7 are given in Table I.

If the two-to-one condition on the areas under the two Lorentz lines is relaxed and the neutron multiplicity is allowed to range between the A and B limits given in Fig. 4, the tantalum data can be fitted with two Lorentz

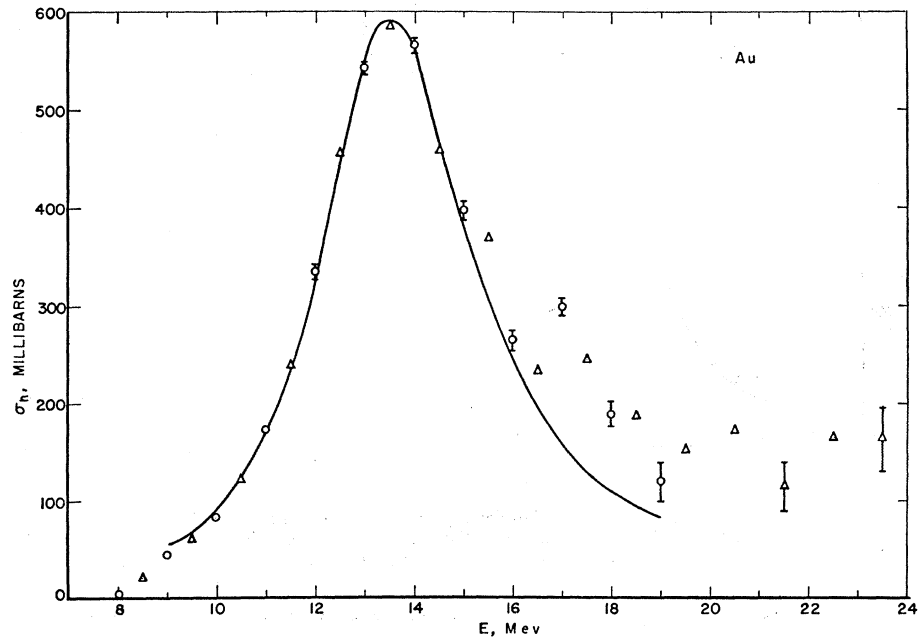

FIG. 7. Neutron cross section for gold. See Fig. 5 for description.

TABLE II. Integral cross sections.

	Tb^{159}	Ta^{181}	Au^{197}
$A\int_0^{24}\sigma_n dE/0.06NZ$	1.27	1.30	1.29
$\int\sigma_b dE/\int\sigma_a dE$	2.00	2.16	1.97
$A\int_0^{\infty}(\sigma_a+\sigma_b)dE/0.06NZ$	1.27	1.35	1.22

lines having a rather large range of parameters. Only the energies of the two lines remain rather well determined. Fits can be obtained to the data with the ratio of the areas under the two peaks ranging anywhere from 1.8 to 3.0. The ratio of the energies of the two resonances, however, ranged only from 1.24 to 1.26. Unless very extreme assumptions are made about the neutron multiplicity for tantalum, it is not possible to obtain a fit to the data given in Fig. 6 with two Lorentz lines for which the area under the lower energy peak is twice that under the high-energy peak. This is the condition which would have to be fulfilled on the hydrodynamical model if the tantalum nucleus were an oblate spheroid.

The areas under the various curves in Figs. 5 to 7 are given in Table II. These areas are all expressed in units of the integrated absorption cross section given by the dipole sum rule for ordinary forces. In this table $\int_0^{24}\sigma_n dE$ is the integral of the actual experimentally determined cross section as plotted in Figs. 5 to 7. The statistical uncertainty in these areas is less than 2%. There is, however, an uncertainty of about 10% in these areas resulting from the uncertainty in the correction made for the neutron multiplicity. In addition, there is a possible error of another 10% resulting from the absolute determination of the efficiency of the neutron detector and the absolute response of the bremsstrahlung monitor. These areas, therefore, are not considered to be known to better than 15%.

Also given in Table II are the ratios of the areas under the two Lorentz lines used to fit the experimental data, and the total area under these two lines, $\int_0^{\infty}(\sigma_a+\sigma_b)dE$. These latter areas are either the same or less than the areas under the experimental points. This probably results to some extent from the use of a wrong neutron multiplicity in correcting the experimental data. There is, however, also some indication that there is absorption at energies above 16 Mev which, on the basis of a hydrodynamical model, would be associated with modes of the nucleus other than those associated with the giant resonance.

The intrinsic quadrupole moment of the nucleus is related to X, the ratio of the major to minor axes of the nucleus, by the expression

$$Q_0=\tfrac{2}{5}Z(a^2-b^2)=\tfrac{2}{5}ZR_0^2A^{\frac{2}{3}}(X^2-1)/X^{\frac{2}{3}}, \qquad (6)$$

TABLE III. Intrinsic quadrupole moments, in barns.

	Tb^{159}	Ta^{181}	Au^{197}
E_b/E_a	1.30±0.05	1.25±0.01	1.06±0.03
$Q_0(R_0=1.09\times10^{-13}$ cm)	5.6 ±0.6	5.7 ±0.3	1.6 ±0.6
Q_0 (Coulomb excitation)	6.9[a]	6.8[a]	2.6[b]

[a] Adler, Bohr, Huus, Mottelson, and Winter, Revs. Modern Phys. **28**, 432 (1956).
[b] P. H. Stelson and F. K. McGowan, Phys. Rev. **99**, 112 (1955).

where R_0 is the constant in the expression for the nuclear radius, $R=R_0A^{\frac{1}{3}}$. Danos[6] has shown that the ratio of the two resonance energies, E_a and E_b, is related to X by

$$E_b/E_a=0.911X+0.089. \qquad (7)$$

Using these expressions and the energies given in Table I, the intrinsic quadrupole moments of these three nuclei have been calculated. These moments are compared with the values obtained from Coulomb excitation in Table III. The two determinations agree within the errors of the measurements. The errors given for the ratio of the resonance energies for each nucleus are estimated on the basis of the various fits that could be obtained to the data given in Figs. 5 to 7 when an approximate two-to-one ratio was required for the area under the high-energy line to that under the low-energy one.

The extension of the simple classical hydrodynamical model of the nucleus as made by Danos to describe the nuclear photoeffect has given a good description of both the shape of the giant resonance and the relation of the splitting of the resonance to the intrinsic quadrupole moment of the deformed nucleus. A splitting of the giant resonance for a deformed nucleus would also be expected to result from a shell-model calculation. Brink[19] has shown that a consistent shell-model calculation of the photoeffect should give the same result as the hydrodynamic model. Such a calculation has not yet been carried out. Those calculations which have been made with shell-model wave functions[20] have not been successful in predicting the shape of the giant resonance.

ACKNOWLEDGMENTS

The authors wish to thank J. E. Leiss and M. Danos for many fruitful discussions. They are indebted to H. K. Skramstad and the staff of the National Bureau of Standards Analog Computer Section as well as to M. Danos for the help they gave both in setting up and carrying out the curve-fitting problem on the computer.

[19] D. M. Brink, Nuclear Phys. **4**, 215 (1957).
[20] J. L. Burkhardt, Phys. Rev. **91**, 420 (1953); S. Rand, Phys. Rev. **107**, 208 (1957); M. Soga and J. Fujita, Nuovo cimento **6**, 1494 (1957).